PROCEEDINGS OF SCIENCE

Advanced Transient Current Technique Systems

G. Kramberger[*†]
Jozef Stefan Institute, Ljubljana, Slovenia
E-mail: Gregor.Kramberger@ijs.si

The Transient Current Technique has been one of the principal tools for studying solid state particle detectors over the last two decades. The basic properties of the system, its components, and signal analysis will be reviewed and examples of its use shown. The Scanning-TCT systems which are based on position resolved carrier generation along the beam with precision of few microns will be presented together with ways of their application as well as a novel way of using Scanning-TCT by utilizing two-photon-absorption for precise three dimensional spatial localization of generated e-h pairs inside the detector.

The 23rd International Workshop on Vertex Detectors,
15-19 September 2014
Macha Lake, The Czech Republic

[*]Speaker.
[†]G. Kramberger is with the Jožef Stefan Institute, Jamova 39, SI-1000 Ljubljana, Slovenia (Tel: (+386) 1 4773512, fax: (+386) 1 4773166,)

© Copyright owned by the author(s) under the terms of the Creative Commons Attribution-NonCommercial-ShareAlike Licence.

PoS(Vertex2014)032

1. Introduction

Transient current technique (TCT) exploits the signal induced in electrodes by the motion of non-equilibrium free carriers in a semiconductor structure. The excitation of free carriers (e-h pairs) can be done in several ways, through pulse biasing, ionizing particles or light pulses. The latter two modalities have been widely exploited in the study of different semiconductor detectors (examples in Refs. [1, 2, 3]). Initially most of the studies were concentrated to the properties of semiconductor materials for which large size pad detectors (tens of mm^2) are very suitable.

CERN R&D collaborations (RD-48, RD-39, RD-42, RD-50) devoted to understanding and improving semiconductor materials used for tracking detectors at LHC, and recently its envisaged upgrade HL-LHC, extensively used TCT for characterization of materials after large fluences of radiation. In the recent years a need emerged not only for probing the material properties, but also identifying the behavior of more complex structures such as multi-electrode detectors. For their studies a focused beam is precisely directed to different points in e.g. pixel and strip detectors.

This work aims to give an introduction to the method and present some of the most typical uses of the technique. It is also intended to equip the reader with some practical advice on constructing and running a TCT setup.

2. Principles and analysis technique

The basic scheme of a TCT system is shown in the Fig. 1. The laser pulse generates e-

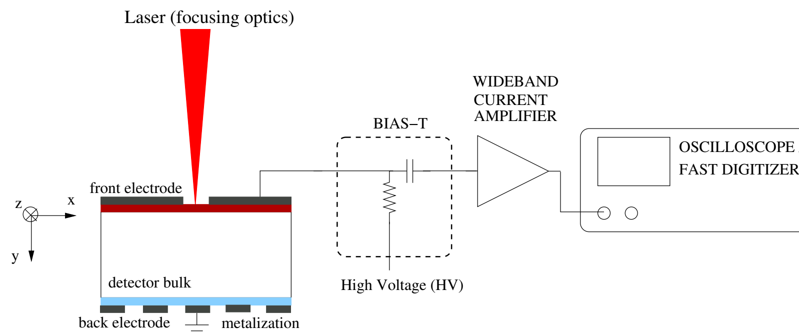

Figure 1: Schematic view of a typical TCT system used for studies of pad detectors.

h pairs in a semiconductor detector. The detector is connected to input of the transimpedance amplifier. Its output is fed to the oscilloscope. There are two ways of connecting the detector to the amplifier. Either back electrode of the detector is at high potential and front electrode at ground or high potential is brought to the front side through so called bias-T which decouples detector bias voltage from the input to the amplifier (AC coupling). The former option has an advantage of avoiding additional components which can distort the signal, but usually results in more complicated grounding scheme as backside of the sensor has to be physically separated from the housing/shielding which protects the sensors from RF pickup. In addition, possible high DC current flowing in the amplifier can influence its response.

PoS(Vertex2014)032

The required speed of components is determined by the investigated structures. Drift velocities in silicon are in the range $10^6 - 10^7$ cm/s [4], which sets the typical time scale of the observed induced currents from ns to few tens ns. This sets the requirements of both laser and electronics. In most state-of-the-art systems the rise time of the measured induced current is determined by the capacitance of the electrode and input impedance of the amplifier. For typical values of 10 pF and 50 Ω the resulting rise times are around 500 ps (*RC*), which requires the bandwidth of the amplifier, bias-T and the oscilloscope/digitizer to be at least of the same order >1 GHz:

- **amplifier**: Wide bandwidth amplifiers are available by many vendors. In most TCT measurements an average response to many laser pulses is taken, thereby diminishing the noise. Large amplification factors allow for lower injected charge, therefore influencing less local electric field in the examined structure. Beside the upper limit of the bandwidth also the lower limit is important as it impacts the shape of the measured pulse, particularly on longer time scales e.g. measurements of detrapping times [5].

- **bias-T**: The bandwidth should match that of the amplifier, however the tolerance to stand high voltages (>1000 V) is often a key property. Already a small impedance mismatch between the cable connecting detector and the input to the bias-T/amplifier leads to reflections which appear also in the measured signal. Usually they can be moved out of the region of interest by using longer cables.

- **laser**: Apart from the wavelength which determines the penetration depth in semiconductor (see Fig. 2 for silicon) the pulse width is crucial. Most TCT systems utilize lasers with pulses shorter than few hundred ps in order to resolve the evolution of pulses from typically few 100 μm thick structure. The frequencies of pulses range from below 1 Hz to several tens of kHz, depending on the desired conditions in the sensor (rate effects, studies of trapping/detrapping). Commercial lasers offer often tunable pulse intensity, but for precise preservation of the laser pulse shape at different intensities the use of neutral density filters (NDF) is a better choice.

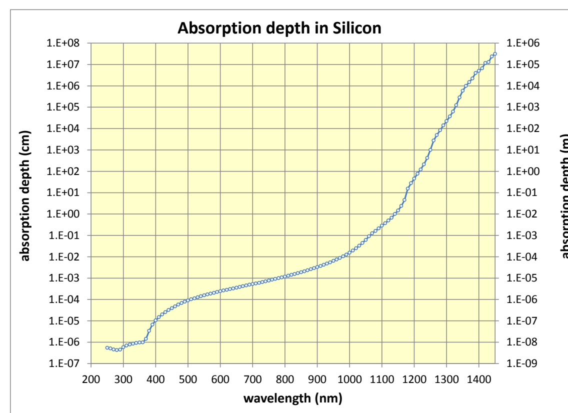

Figure 2: Absorption depth of the light in intrinsic silicon at 300 K (taken from Ref. [6]).

PoS(Vertex2014)032

2.1 Signal analysis

The measured current pulse I_m is a convolution of three different functions, induced current I in the detector electrode, transfer function of the electronics T and the shape of the laser pulse P

$$I_m(t) = \int\int T(t-t^{'}) \cdot I(t^{'}-t^{''}) \cdot P(t^{''})\, dt^{''}\, dt^{'} \qquad . \tag{2.1}$$

In general the extraction of I from the Eq. 2.1 is a complex task. However, in many cases T is dominated by the input impedance of the amplifier (R) and capacitance of the sample (C), and the laser pulse is much shorter than τ_{RC}, which means:

$$T(t) = \frac{A}{\tau_{RC}} exp(-\frac{t}{\tau_{RC}}) \quad , \quad P(t) = B\delta(t) \quad , \tag{2.2}$$

where $\tau_{RC} = RC$, A amplification assumed to be constant over the bandwidth and B laser pulse amplitude expressed in number of generated e-h pairs. By inserting Eq. 2.2 in Eq. 2.1 the solution of I can be obtained in the time domain as

$$I = \frac{1}{AB}\left[\tau_{RC}\frac{dI_m}{dt} + I_m\right] \quad . \tag{2.3}$$

If both τ_{RC} and laser pulse are shorter than the required time resolution of the measurement the Eq. 2.3 simplifies to $I(t) \approx \frac{1}{AB} I_m(t)$.

2.2 Induced current

The detector properties can be extracted from the current induced by the motion of the charge q in the electric field $\vec{E}$, which is given by Ramo's theorem [7, 8] as

$$I_{e,h}(t) = q\, \vec{v}(\vec{r}(t)) \cdot \vec{E_w}(\vec{r}(t)) = N_{e,h}\, \exp(\frac{-t}{\tau_{eff,e,h}})\, \mu_{e,h}\, \vec{E(\vec{r})} \cdot \vec{E_w}(\vec{r}) \tag{2.4}$$

where $\vec{r}$ is the location of the charge (either of e or h indicated by subindices), $\vec{v}$ its velocity, μ mobility and $\vec{E_w}$ the weighting field given by the electrode configuration in the detector. The full implications of the Eq. 2.4 would largely exceed the scope of this work and can be found in Ref [9].

2.3 Examples of measurements

In its simplest form for pad detectors, which are commonly used to study the material properties, the Eq. 2.4 reduces to a single dimension with $E_w = 1/W$,

$$I_{e,h}(t) = N_{e,h}\, \exp(\frac{-t}{\tau_{eff,e,h}})\, \frac{1}{W}\, \mu_{e,h} E \quad . \tag{2.5}$$

Examples of measured current pulses are shown in Fig. 3. There are several key detector properties that can be extracted from the pulse shapes:

- Sign and the concentration of the space charge : decrease/increase of the velocity during the movement of the charge is related to the changes in electric field strength, which in turn is related to the space charge. See for example Fig. 3a,b,c for a non-irradiated detector of constant positive space charge and a case of opposite space charge at both detector sides for an irradiated MCz detector ("double junction" effect [10]).

PoS(Vertex2014)032

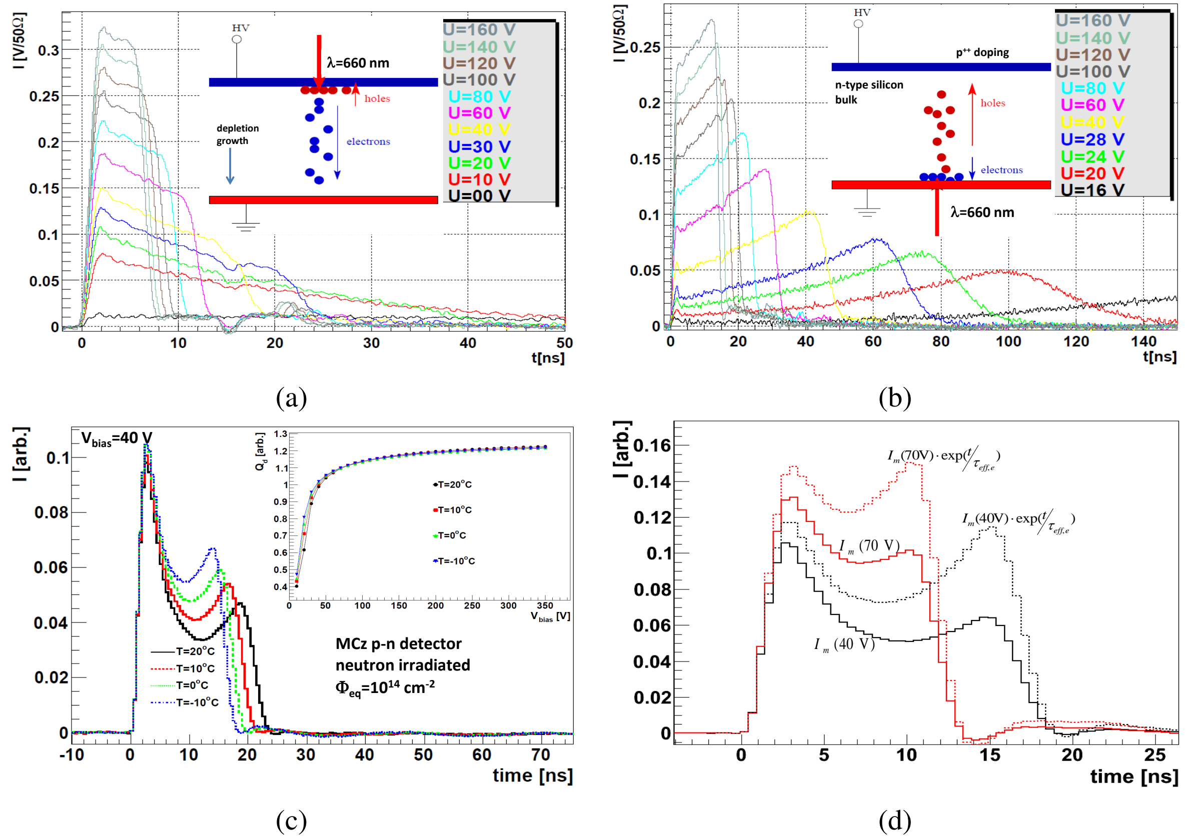

Figure 3: Current pulse shapes in a non-irradiated p-n pad detector with $V_{fd} \approx 20$ V after illumination with red light; (a) front-illumination - current pulses due to drift of electrons and (b) back illumination - current pulses are due to drift of holes. (c) Current pulses at 40 V for a neutron irradiated silicon MCz p-n detector at different temperatures after front illumination. Charge collection in 60 ns at different bias voltages is shown in the the inset (taken from Ref. [5]) (d) Current pulses at 40 V and 70 V for the detector shown in (c) and the corrected pulses for the exponential term with $\tau_{eff,e} = 26$ ns that yields equal charge.

- Full depletion voltage : if the detector is fully depleted the current pulse ends after the end of drift which can be seen as a knee in the induced current pulse (e.g. at 22 ns for 30 V in Fig. 3a). In a non-depleted device the current asymptotically approaches $I_m = 0$ as shown for 10 V.

- Induced charge $Q = \int_0^{t_{int}} I(t)dt$: it is difficult to achieve always the same intensity and illumination spot therefore the charge Q is usually given relatively with respect to the other voltages only. See the inset of Fig. 3c for the dependence of Q on V_{bias} for different voltages.

- Trapping of the drifting charge [11, 12, 13, 14] : $Q(V)$ plot in Fig. 3c shows that $Q(V_{bias} > V_{fd} \approx 40$ V) increases due to shorter drift and less trapping. If the induced currents measured at different voltages are corrected for the term $\exp(t/\tau_{eff,e,h})$ the integral of corrected pulses - corrected charge - should be the same at all voltages above V_{fd}. As an example of pulses corrected by effective trapping term for two different voltages is shown in Fig. 3d.

- Mobility measurements : in cases where space charge is small the velocity doesn't change

PoS(Vertex2014)032

much over the entire detector thickness. The mobility of the carrier type can be extracted from the drift time t_{drift} of carriers generated close to the surface: $\mu_{e,h} \approx \frac{W^2}{V_{bias} t_{drift,e,h}}$. The pulses shown in Fig. 3a,b serve as good examples.

3. Scanning-TCT and multielectrode system

The study of segmented detectors/structures requires the beam to be narrower than the size of the investigated feature. In recent years Scanning-TCT systems emerged [15, 16, 17], which utilize optical system (see Fig. 4) to achieve a beam spot size of few μm (FWHM). The optical system and detector mounting table are placed on movable stages thus forming a full 3D translation system. In order to achieve a small spot size a single mode optical fibers with core dimension of only 4 μm are usually used. A special attention should be paid to the spot sizes of light with small penetration depth. Free carrier concentrations can easily reach levels comparable with the doping levels therefore significantly altering local space charge and electric field (plasma effects).

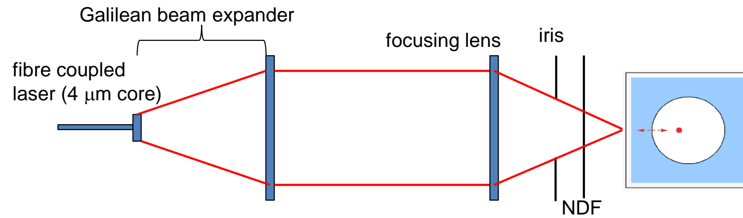

Figure 4: Schematic view of the optical system.

In multielectrode systems it is important to connect the electrodes to the impedances that correspond to those during normal operation. If this is not the case, E_w in Eq. 2.4 can be different for both uses and the measurements can be misinterpreted. As best example serve AC coupled silicon strip detectors. The segmented implants are connected through high resistance (polysilicon resistors) to the DC bias, but the measured induced currents are different when a single/investigated Al strip is connected to low impedance with other strips floating and when all Al strips are connected to low impedance (see Ref [18]).

Another example is the use of several amplifiers (sometimes called multi-channel TCT) connected to different electrodes at the same time, where similar input impedances of the amplifiers are required.

3.1 Top-TCT

The use of Scanning-TCT when surface of the planar or so called 3D detectors [19] is illuminated is referred to as top-TCT. It is used to determine the properties of the silicon detector surface [20] utilizing red light as well as the properties of charge collection similar to that of the minimum ionizing particle by an infrared laser [18].

An example of Top-TCT measurement in an irradiated silicon strip detector can be seen in Fig. 5a, where the charge induced in the strip connected to the amplifier is shown for different positions of the illumination spot. Negative charges induced in the neighbors due to trapping [21], can be

PoS(Vertex2014)032

clearly seen. A similar measurement shown in Fig. 5b was performed in special diode with short strips ganged together on one side (spaghetti diode) and not fully metallized strips on the other. At high voltages the most efficient region is not under the strips but at the implant edges where the electric field is higher and by that also multiplication of the charge by impact ionization.

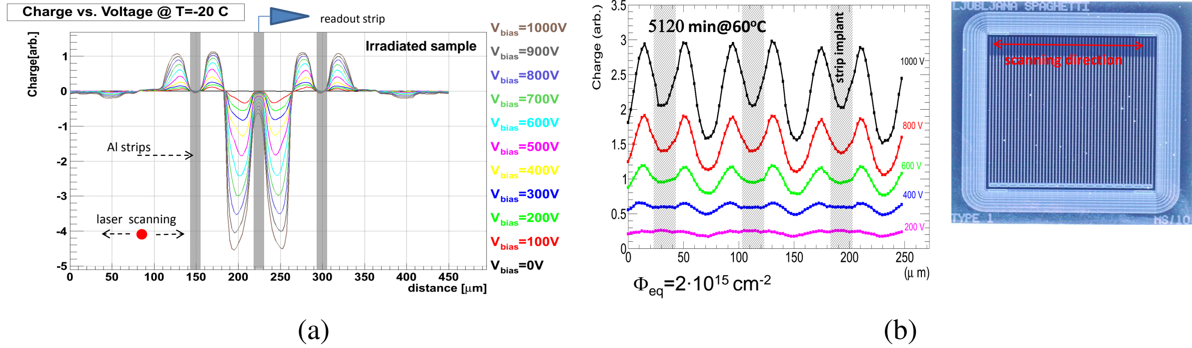

(a) (b)

Figure 5: Charge collection profile perpendicular to the strips of an irradiated: (a) silicon strip detector and (b) "spaghetti diode". Al strips reflect the light and the measured charge vanishes. The strips are not fully metallized for the spaghetti diode (top part in the figure) thus allowing light injection underneath the implant (taken from Ref. [18]).

3.2 Edge-TCT

The properties of the detector bulk can be extracted from from the time evolution of the pulse (Eq. 2.4). There are two obstacles in this procedure; the current at a given time is not easily transferred to current at a given position of the moving carriers. Moreover in case of severe trapping the exponential term dominates and damps the current to the level of noise.

An alternative approach is based on illumination of the detector's edge by the light of long penetration depth. Such an approach requires polishing of the edge in order to minimize diffraction of the light inside the sensor. The schematic layout for a strip sensor is shown in Fig. 6. As the carriers are generated at a given depth of the detector the initial movement of the carriers reveals the strength of the electric field at the point of their creation as it follows from Eq. 2.4. The weighting field term for illumination in direction perpendicular to the strips results in effective factor of $1/W$ which simplifies the analysis [22].

There are several useful information that can be extracted from the waveforms (see Ref. [22]). One of the most investigated quantity is the drift velocity at given position of the beam (y) which is extracted from the measured induced current. Immediately after illumination ($t \sim 0$) $\exp(-t/\tau_{eff,e,h}) \approx 1$ and Eq. 2.4 gives

$$I(y,t \sim 0) = I_e + I_h \approx e_0 N_{e,h} \frac{v_e(y) + v_h(y)}{W} \quad . \tag{3.1}$$

Eq. 3.1 tells that the current measured immediately after light injection is proportional to the sum of both drift velocities, regardless of the trapping times.

The illumination of strips along the strips/electrodes is more appropriate for studies of charge sharing, charge multiplication profiles or the effects of the weighing field on charge collection [23].

PoS(Vertex2014)032

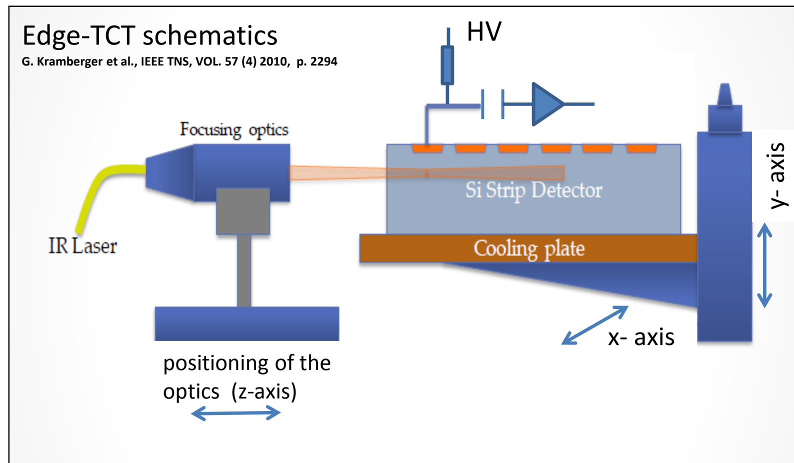

Figure 6: Schematic view of the Edge-TCT technique.

Some examples Edge-TCT measurements can be seen in Fig. 7. The observation of the charge multiplication due to impact ionization in a strip detector is shown in Fig. 7a. The appearance of the second peak in induced current is attributed to the arrival of the electrons to the strips where the fields are large enough for impact ionization . The holes produced drift away from the strips and give rise to the second peak, which is not observed at lower voltages. Extracted velocity profiles in heavily irradiated silicon strip detector, shown in Fig. 7b, reveal the presence of the electric field in the entire thickness of the detector already at relatively low voltages [24]. The profiling of the charge collection in a 3D strip detector is shown in Fig. 7c. The regions of high and low charge collection efficiency can be clearly identified.

4. Future systems : TPA - TCT

Although a combination of Edge-TCT and Top-TCT allows for determining charge collection properties of different detector regions it requires substantial effort. Ideally, the charge deposition would be localized only in the desired region of interest and not all along the beam. In that way it would be directly possible to map charge collection of complex 3D structures. This can be achieved by using a two-photon-absorption (TPA), where a single electron in the valence band is excited by the two photons each having energy lower than the band-gap. To achieve conditions for TPA the 100 fs laser pulse is focused to few μm [26]. The probability of the TPA depends quadratically on concentration of photons leading to the deposition of the charge only at the waist of the Gaussian beam as can be seen in Fig. 8a. The first measurements with the technique were performed with promising results [27]. An example of simulated and measured induced currents is shown in Fig. 8b. A very good agreement between the two proofs the precise localization of the generated charge.

The TPA competes with generation of e-h pairs by single photon absorption in semiconductors with large concentration of energy levels in the band-gap. The excitation of carriers from those require smaller photon energy. Typically irradiated semiconductor detectors have large concentration

PoS(Vertex2014)032

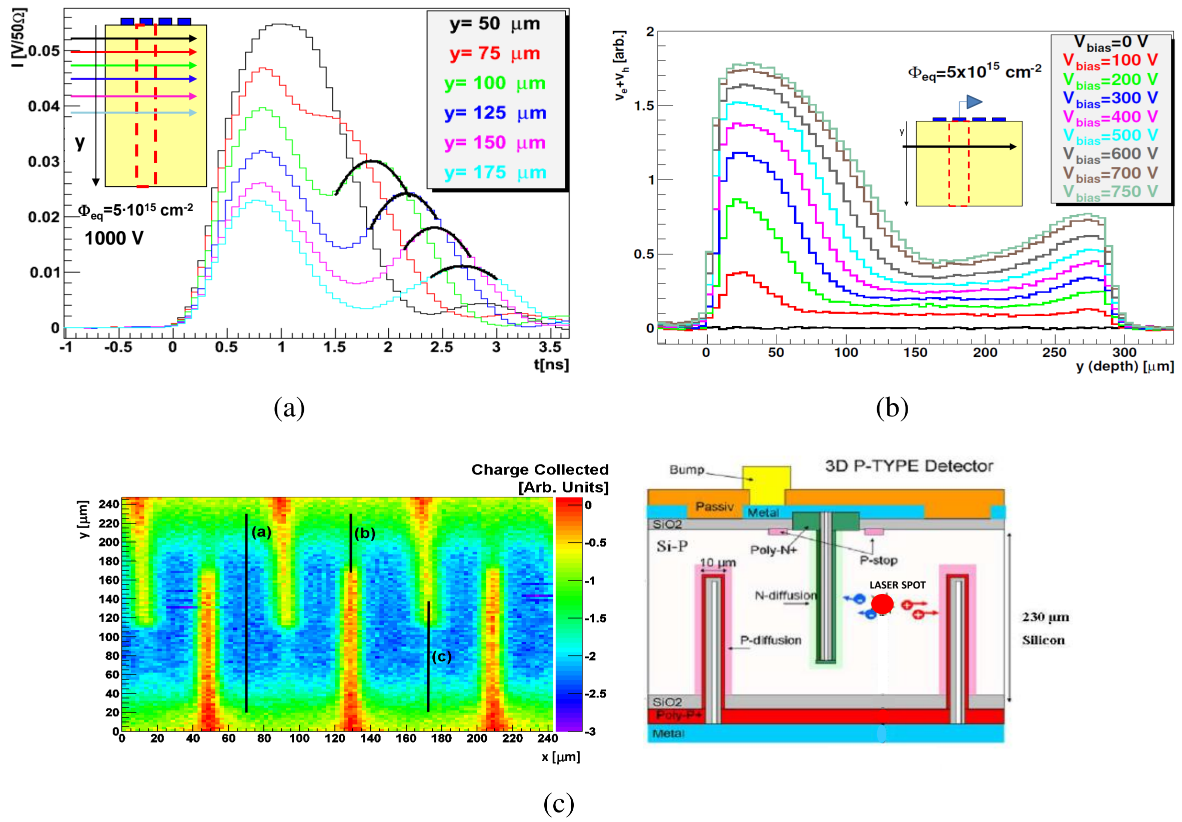

Figure 7: Example of Edge-TCT measurements: (a) Induced current pulses corresponding to charge multiplication in heavily irradiated silicon strip detector at 1000 V (from Ref. [22]), (b) velocity profile in heavily irradiated silicon strip detector (from Ref. [24]), (c) profiling of the charge collection in a 3D strip detector (from Ref. [25]).

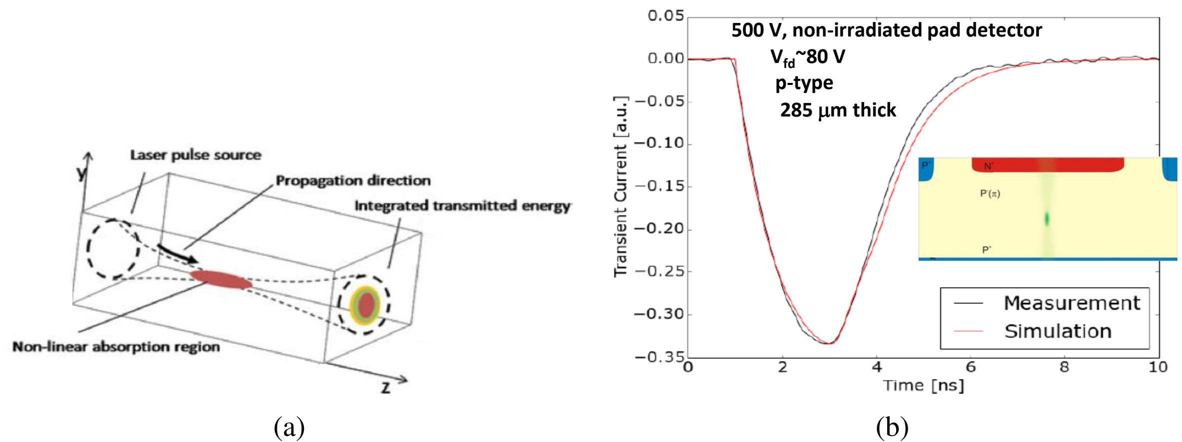

Figure 8: (a) Schematic view of the beam profile and region with TPA process (from Ref [26]). (b) Measured and simulated induced currents in a silicon pad detector with TPA generation of e-h pairs in the center of the detector (from Ref [27]).

PoS(Vertex2014)032

of energy levels in the band-gap therefore a careful optimization of operation parameters and signal analysis will be required.

5. Conclusions

The Transient Current Technique has evolved in the last decades as one of the main tools to characterize semiconductors detectors. Initially it was used to determine material properties, but in recent years the Scanning-TCT is used also to study properties of segmented detectors and in many ways complements the test-beam measurements. The use of scanning TCT revealed properties of heavily irradiated silicon detector, such as charge multiplication, drift velocity profiles, trapping, which would be extremely difficult to study without it. A new step forward in the evolution of TCT systems is the two photon absorption TCT, where the induced current can be measured from any voxel of few tens μm^3 in the detector.

References

[1] V. Eremin, N. Strokan, E. Verbitskaya, Z. Li, "Development of transient current and charge techniques for the measurement of effective net concentration of ionized charges (N-eff) in the space charge region of p-n junction detectors”, Nucl. Instr. and Meth. A 372 (1996) p. 388.

[2] J. Fink, H. Kruger, P. Lodomez, N. Wermes, ”Characterization of charge collection in CdTe and CZT using the transient current technique”, Nucl. Instr. and Meth. A 560 (1996) p. 435.

[3] J. Haerkoenen, V. Eremin, E. Verbitskaya, S. Czellara, P. Pusac, Z. Lid, T.O. Niinikoskie, ”The Cryogenic Transient Current Technique (C-TCT) measurement setup of CERN RD39 Collaboration”, Nucl. Instr. and Meth. A 581 (2007) p. 347.

[4] C. Canali, G. Ottavian, A. Alberigi, “Drift velocity of electrons and holes and associated anisotropic effects in silicon”, *J. of Phys. Chem. Solids*, Vol. 32 (1971), p. 1707.

[5] G. Kramberger, V. Cindro, I. Mandić, M. Mikuž, M. Zavrtanik, ”Determination of detrapping times in semiconductor detectors”, JINST 7 (2012) P04006.

[6] M.A. Green and M. Keevers, "Optical properties of intrinsic silicon at 300 K ", Progress in Photovoltaics Vol. 3(No. 3) (1995) p. 189.

[7] S. Ramo, “Currents Induced by Electron Motion”, Proceedings of I.R.E. 27 (1939) p. 584.

[8] E. Gatti, G. Padovini, V. Radeka, "Signal evaluation in multielectrode radiation detectors by means of a time dependent weighting vector”, Nucl. Instr and Meth. 193 (1982) p. 651.

[9] G. Kramberger, “Signal formation in irradiated silicon detectors”, PhD. Thesis, University of Ljubljana, CERN-THESIS-2001-038 (2001).

[10] V. Eremin, E. Verbitskaya, Z. Li, ”The origin of double peak electric field distribution in heavily irradiated silicon detectors”, Nucl. Instr. and Meth. A 476 (2002) p. 556.

[11] T.J. Brodbeck, A. Chilingarov, T. Sloan, E. Fretwurst, M. Kuhnke, G. Lindstroem, “A new method of carrier trapping time measurment”, Nucl. Instr. and Meth. A455 (2000) p. 645.

[12] G. Kramberger, V. Cindro, I. Mandić, M. Mikuž, M. Zavrtanik, ”Determination of effective trapping times for electrons and holes in irradiated silicon”, Nucl. Instr. Meth. A 476 (2002) 645.

PoS(Vertex2014)032

[13] G. Kramberger, V. Cindro, I. Mandić, M. Mikuž, M. Zavrtanik, "Effective trapping time of electrons and holes in different silicon materials irradiated with neutrons, protons and pions", Nucl. Instr. and Meth. A 481 (2002) p. 297.

[14] O. Krasel, C. Gossling, R. Klingenberg, S. Rajek, R. Wunstorf, ”Measurement of trapping time constants in proton-irradiated silicon pad detectors”, IEEE Trans. Nucl. Sci. 51(1) (2004) p. 3055.

[15] G. Kramberger et al., "Position sensitive TCT measurements with 3D-sct detectors", Presented at 8th RD50 Workshop, Prague, 25-28.6.2006.

[16] N. Pacifico et al., "Edge TCT and Charge Collection Efficiency study on pion irradiated n-on-p strips", Presented at 18th RD50 Workshop, Liverpool, 23-25.5.2011.

[17] J. Becker, D. Eckstein, R. Klanner, G. Steinbrueck, "Impact of plasma effects on the performance of silicon sensors at an X-ray FEL", Nucl. Instr. and Meth. A 615 (2010) p. 230.

[18] I. Mandić, V. Cindro, A. Gorišek, M. Mikuž, M. Milovanovič, M. Zavrtanik , “TCT measurements of irradiated strip detectors with a focused laser beam”, JINST 8 (2013) P04016.

[19] S. Parker, C.J. Kenny, J. Segal, ”3D - A proposed new architecture for solid-state radiation detectors”, Nucl. Instr. and Meth. A 395 (1997) p. 328.

[20] T. Pohlsen, J. Becker, E. Fretwurst, R. Klanner, J. Schwandt, J.Zhang, ”Study of the accumulation layer and charge losses at the Si-SiO2 interface in p(+)n-silicon strip sensors", Nucl. Instr. and Meth. A 721 (2013) p. 26.

[21] G. Kramberger, V. Cindro, I. Mandić, M. Mikuž, M. Zavrtanik, "Influence of Trapping on Silicon Microstrip Detector Design and Performance", IEEE Trans. Nucl. Sci. Vol. 49(4), 2002, p. 1717.

[22] G. Kramberger, V. Cindro, I. Mandić, M. Mikuž, M. Milovanovič, M. Zavrtanik, K. Žagar, ”Investigation of Irradiated Silicon Detectors by Edge-TCT “, IEEE Trans. Nucl. Sci. Vol. 57(4), 2010, p. 2294.

[23] I. Mandić et al., "E-TCT with laser beam directed parallel to strips", Presented at 25th RD50 Workshop, CERN, Geneve, 17-19.11.2014.

[24] G. Kramberger, V. Cindro, I. Mandić, M. Mikuž, M. Milovanovič, M. Zavrtanik, "Modeling of electric field in silicon micro-strip detectors irradiated with neutrons and pions", JINST, Vol. 9 (2014) P10016.

[25] G. Stewart, C. Fleta, G. Kramberger, M. Lozano, M. Milovanović, G. Pellegrini, “Analysis of edge and surface TCTs for irradiated 3D silicon strip detectors", JINST, Vol. 8 (2013) P03002.

[26] R. P. Pinto et al.,”Two Photon Absorption and carrier generation in semiconductors", Presented at 25th RD50 Workshop, CERN, Geneve, 17-19.11.2014.

[27] I. Vila et al., ”TPA-TCT: A novel Transient Current Technique based on the Two Photon Absorption (TPA) process", Presented at 25th RD50 Workshop, CERN, Geneve, 17-19.11.2014.

PoS(Vertex2014)032